RESEARCH ARTICLE

Special Section:

The Southern Ocean Carbon and Climate Observations and Modeling (SOCCOM) Project: Technologies, Methods, and Early Results

Key Points:
- OSSEs for the SOCCOM array estimate the skill of reconstructing maps of biogeochemical tracers from float profiles in the Southern Ocean
- The reconstruction skill depends on the magnitude of the seasonal cycle, mesoscale variability, and spatial gradients
- Movement and number of floats are important, and an array size of 150 floats is a reasonable choice for the Southern Ocean

Correspondence to:
I. Kamenkovich,
ikamenkovich@miami.edu

Observing System Simulation Experiments for an array of autonomous biogeochemical profiling floats in the Southern Ocean

Igor Kamenkovich[1] (iD), Angelique Haza[1] (iD), Alison R. Gray[2,3] (iD), Carolina O. Dufour[2,4] (iD), and Zulema Garraffo[5] (iD)

[1]RSMAS, University of Miami, Miami, Florida, USA, [2]Program in Atmospheric and Oceanic Sciences, Princeton University, Princeton, New Jersey, USA, [3]Now at School of Oceanography, University of Washington, Seattle, Washington, USA, [4]Now at Department of Atmospheric and Oceanic Sciences, McGill University, Montreal, Quebec, Canada, [5]IMSG at NOAA/EMC, College Park, Maryland, USA

Abstract This study uses Observing System Simulation Experiments (OSSEs) to examine the reconstruction of biogeochemical variables in the Southern Ocean from an array of autonomous profiling floats. In these OSSEs, designed to be relevant to the Southern Ocean Carbon and Climate Observation and Modeling (SOCCOM) project, the simulated floats move with oceanic currents and sample dissolved oxygen and inorganic carbon. The annual mean and seasonal cycle of these fields are then reconstructed and compared to the original model fields. The reconstruction skill is quantified with the reconstruction error (RErr), defined as the difference between the reconstructed and actual model fields, weighted by a local measure of the spatiotemporal variability. The square of the RErr is small ($<$0.5) for 150 floats in most of the domain, which is interpreted to mean that the reconstruction skill is high. An idealized analytical study demonstrates that the RErr depends on the magnitude of the seasonal cycle, spatial gradients, speed of float movement, amplitude of mesoscale variability, and number of floats. These factors explain a large part of the spatial variability in the RErr and can be used to predict the reconstruction skill of the SOCCOM array. Furthermore, our results demonstrate that an array size of 150 floats is a reasonable choice for reconstruction of surface properties and annual-mean 2000 m inventories, with the exception of the seasonal cycle in parts of the Indo-Atlantic, and that doubling this number to 300 results in a very modest increase in the reconstruction skill for dissolved oxygen.

1. Introduction

The Southern Ocean Carbon and Climate Observation and Modeling (SOCCOM) biogeochemical array has started providing a wealth of data with the goal of quantifying the role of the Southern Ocean in the global carbon cycle. The project aims to deploy 150–200 autonomous floats that take vertical profiles of dissolved oxygen (O_2), nitrate, pH, and chlorophyll concentrations in the upper 2000 m every 10 days. The spatial and temporal sampling coverage of the biogeochemical data will be unprecedented but may still be too sparse for accurate resolution of fields in the regions of sharp fronts and strong temporal variability. Quantitative analysis is thus needed to assess the skill with which large-scale gridded properties can be reconstructed from these sparse local observations, to establish where in the domain this skill is the highest, and to determine which temporal and spatial features the float array is able to reveal. In making decisions about the size of the observational array, it is important to balance improvements in the accuracy of the reconstructed fields against increased costs of the array. The conclusions from an analysis of the reconstruction skill can therefore be used to optimize the deployment strategy, informing decisions on how many profiling floats to deploy and where to deploy them.

The reconstruction skill is determined by the temporal and spatial variability in the sampled fields and by the number, location, and frequency of the profiles. This dependence is complicated, since the floats are constantly moving, sampling different parts of the ocean at different times. These issues can be effectively addressed by Observing System Simulation Experiments (OSSEs) [*Arnold and Dey*, 1986]. The technique has been used to analyze different ocean observing systems in ocean models of varying complexity [e.g., *Kindle*,

1986; *Barth and Wunsch*, 1990; *Bennett*, 1990; *Hernandez et al.*, 1995; *Hackert et al.*, 1998; *Schiller et al.*, 2004; *Ballabrera-Poy et al.*, 2007; *Vecchi and Harrison*, 2007; *Griffa et al.*, 2006]. In the setting relevant to SOCCOM, float trajectories can be either simulated in a numerical model or taken from an existing profiling float array (Argo, http://www.argo.ucsd.edu) and then used to sample a model-simulated field the way that the real floats sample the real ocean. After reconstructing the field from the resulting synthetic data, the reconstruction skill can be readily quantified using a convenient metric—the reconstruction error, defined as the difference between the reconstructed and model fields [*Kamenkovich et al.*, 2009, 2011]. The advantages of this method are in the precise knowledge of the model fields and in the ability to estimate the dependence of the reconstruction skill on the number of floats, deployment locations, and other parameters of the SOCCOM array.

Several factors can impact the reconstruction skill. Sampled fields have complex spatial structure with a range of temporal scales, which can affect the reconstruction skill of climatological values in complicated ways. For example, the strong Antarctic Circumpolar Current (ACC) significantly displaces profiling floats during the 10 day sampling interval. As demonstrated by *Kamenkovich et al.* [2009], this displacement can complicate reconstruction of the time-dependent oceanic state and even lead to gaps in the spatial sampling coverage. Furthermore, advection by powerful mesoscale eddies, which have velocities that often greatly exceed the velocity of the time-mean circulation, can change spatial distribution of floats. The overall spatial coverage can be expected to become more uniform, which can improve reconstruction accuracy [*Kamenkovich et al.*, 2011], but float divergence can also take place, leading to reduced coverage in some regions.

In this study, we examine the reconstruction skill for biogeochemical quantities by an array of profiling floats in the Southern Ocean. As in any OSSE, applicability of our results to the actual observing system is contingent on how closely the numerical simulation represents the real ocean. Previous attempts to quantify the number of floats needed to reconstruct biogeochemical quantities and the associated reconstruction skill have been carried out with coarse-resolution models and fixed (not moving) floats [*Majkut et al.*, 2014]. Our study extends this analysis into a more realistic setting with moving floats and high-resolution numerical simulations. Despite the use of high-resolution state-of-the-art models, the model statistics can still be different from the real ocean. We begin by presenting an analytical study ("idealized OSSE," section 2) that explores the sensitivity of the reconstruction skill to various factors, which will be useful in interpreting the results of comprehensive OSSEs. Section 3 describes the full comprehensive OSSEs, which are carried out using state-of-the-art high-resolution models with a sampling strategy closely resembling the Argo and SOCCOM methodology. In section 4, we analyze the resulting reconstructed monthly climatology of dissolved oxygen (O_2) and dissolved inorganic carbon (DIC), focusing on the dependence of the reconstruction skill for O_2 on the spatial scale and on the number of floats. DIC is not measured directly by the SOCCOM array but is derived from the measured variables (temperature, salinity, nitrate, O_2, and pH). We include DIC in this study because one of SOCCOM's main goals is to estimate the carbonate system in the Southern Ocean. Conclusions are drawn in section 5.

2. Idealized OSSE

The most important factors affecting the reconstruction skill are the spatiotemporal variability in the sampled field, the movement of floats, and the number of floats [*Kamenkovich et al.*, 2009]. Understanding this dependence is challenging in a comprehensive OSSE because of strong geographical variations in all of these factors. Prior to the analysis of the full comprehensive OSSEs, we examine the importance of these factors by designing an idealized analytical study. Our main objective here is to understand how the reconstruction skill depends on the length scale in the signal and on such parameters as the magnitude of the seasonal cycle, mesoscale variability, and float movement. For this purpose, we consider a tracer varying with time t and distance x in a periodic domain of length L, and decompose this field into a set of Fourier harmonics with spatial length scales $L_n = L/n$ and amplitude C_n:

$$F(x, t) = \sum_{n=0}^{n_{max}} C_n \cos\left(\frac{2\pi nx}{L}\right)\left(1 + A\sin\frac{2\pi t}{T}\right) \qquad (1)$$

$F(x, t)$ represents a climatological signal with a seasonal cycle of amplitude A. We take $T = 1$ year, $L = 20,000$ km and vary n between 0 and $n_{max} = 50$. To make further progress, we examine reconstruction

of the sum of the basin-scale (x-independent) part of the signal and the nth harmonic. To study the impacts of mesoscale variability on the reconstruction of each harmonic, we also add an idealized mesoscale signal, in the form of waves with amplitude B and length scale L_e, propagating at speed c:

$$F(x,t) = \left(1 + \frac{C_n}{C_0}\cos\left(\frac{2\pi n x}{L}\right)\right)\left(1 + A\sin\frac{2\pi t}{T}\right) + B\sin\frac{2\pi}{L_e}(x - ct) \tag{2}$$

For this study, we take $L_e = 100$ km and $c = L_e/30$ days ≈ 0.04 m s^{-1}, which are reasonable choices for the ACC region. Note that the monthly average of this mesoscale term is exactly zero.

The field (2) was sampled by N "floats" moving with constant speed U for 1 year. Data samples are taken every 10 days, with start dates of the floats staggered throughout the first 10 days and initial positions of all floats randomly distributed. The reconstruction of the monthly values of F in this idealized OSSE is carried out with a simple linear interpolation in x-direction. To compute the monthly fields, all measurements within the same month are clustered together. The reconstruction error in the annual-mean field (RErr$_a$) is defined as

$$\text{RErr}_a = \frac{\sqrt{2}C_0}{C_n}\left\langle\left(\left(\frac{1}{12}\sum_{m=1}^{12}\widehat{F_m}\right) - \left(1 + \frac{C_n}{C_0}\cos\left(\frac{2\pi n x}{L}\right)\right)\right)^2\right\rangle^{\frac{1}{2}} \tag{3}$$

The reconstruction error for the seasonal cycle is defined as

$$\text{RErr}_s = \frac{1}{W^{1/2}}\left\langle\sum_{m=1}^{12}\left\{\widehat{F_m} - \left(\frac{1}{12}\sum_{m=1}^{12}\widehat{F_m}\right) - AS_m\left(1 + \frac{C_n}{C_0}\cos\left(\frac{2\pi n x}{L}\right)\right)\right\}^2\right\rangle^{1/2}$$

$$W = \left(\sum_{m=1}^{12}(AS_m)^2\right)\left(1 + \frac{C_n^2}{2C_0^2}\right) \tag{4}$$

where $\widehat{F_m}$ is the reconstructed field for month m, $S_m = \sin\frac{2\pi t}{T}$ averaged over month m, and angle brackets indicate spatial averaging. Note that both reconstruction biases are weighted by the standard deviation in the signal, and that their squares can be interpreted as normalized mean squared reconstruction bias. In the rest of this section, we will analyze the dependence of RErr$_a^2$ and RErr$_s^2$ on $L_n = L/n$, N, U, A, and B. We set $C_n/C_0 = 0.5$, and verified that other values do not change the sensitivity of RErr to parameters qualitatively.

To study the sensitivity of the reconstruction skill to the average spacing between floats, we set $U = 0.05$ m s^{-1}, which is an appropriate choice for the ACC at 1 km depth [e.g., *Nowlin and Klinck*, 1986]. In the real ocean, U can be interpreted as the difference between the propagation speed of tracer anomalies at, for example, the surface and movement of the floats at 1000 m depth. Guided by the analysis of the full OSSEs (see section 3.1), we set $A = 0.35$, and $B = 0.2$ and vary the number of floats N. As expected, RErr$_a$ and RErr$_s$ increase with decreasing N (Figure 1). The increase, however, depends on the length scale L_n that is being reconstructed (Figures 1c and 1d). For L_n less than approximately $5L/N$, RErr$_s^2$ is >0.5, which means that the absolute error variance is greater than half the variance in the monthly values and thus the reconstruction skill is deemed low. This result suggests that at least five data points are needed for resolving each length scale in a monthly climatology. As long as a length scale is resolved, the RErr is largely insensitive to the number of floats, e.g., for $L_n = 5000$ km and profile spacing < 1000 km in Figure 1d. Note, however, that a large number of floats are needed to bring RErr$_s$ close to zero (Figures 1b and 1d), because of the need to have multiple measurements within the same month to produce a meaningful monthly mean.

The dependence of RErr on float movement U and magnitude of time dependence (A and B) is summarized in Figure 2 for $N = 30$ and $L_n = 4000$ km. *Kamenkovich et al.* [2009] discussed "positive" (increase in the sampling coverage) and "adverse" (distortion of the seasonal cycle) effects of float movement. The positive effect explains the decrease in RErr$_a$ with increasing U (Figure 2a). The adverse effect is dominant for $U < 0.1$ m s^{-1}, with the smallest RErr$_s$ found for $U = 0$ [see also *Kamenkovich et al.*, 2009]. The positive effect balances the adverse one for $U > 0.1$ m s^{-1} and further increases in U lead to nearly constant RErr$_s$.

For the reconstruction of the seasonal cycle, the magnitude of the seasonal cycle A has only a slight effect on the absolute mismatch between the actual and reconstructed fields, (A^2RErr$_s^2$, red line in Figure 2b), so that RErr$_s^2$ decreases sharply with larger A (blue line in Figure 2b). This dependence is most pronounced for
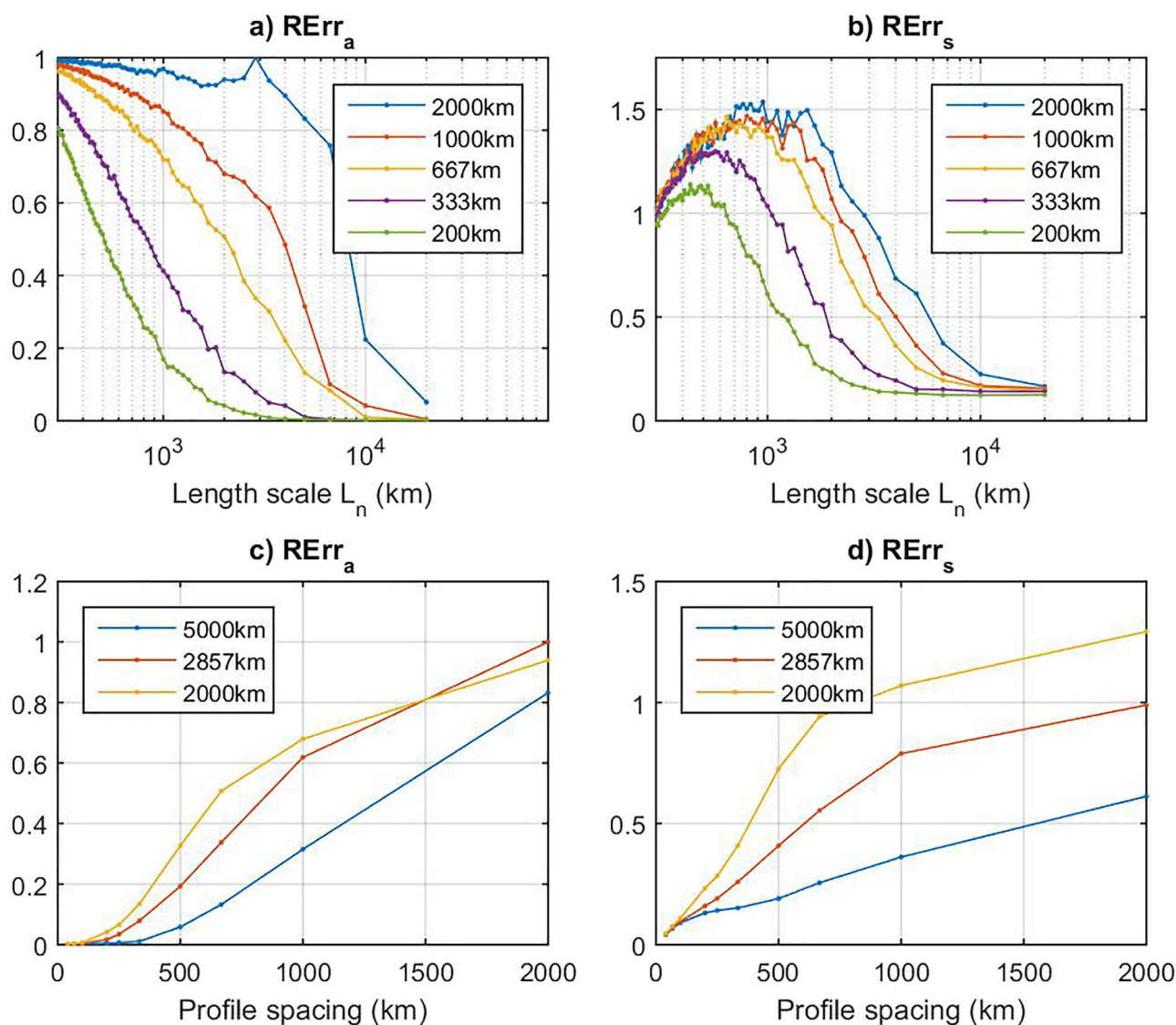
Figure 1. Dependence on the number of floats N in the idealized OSSEs. (top row) RErr as a function of logarithm of the length scale L_n for five different values of profile spacing L/N (shown by different colors) for the (a) $RErr_a$ and (b) $RErr_s$. (bottom row) RErr as a function of the profile spacing for three different values of L_n (shown by different colors) for the (c) $RErr_a$ and (d) $RErr_s$.

very long L_n (not shown), for which the absolute mismatch is insensitive to A. This behavior is observed for all values of parameters, as long as there is spatial and mesoscale variability in the signal ($n \neq 0$ and $B \neq 0$). For $n = 0$ and $B = 0$ (not shown), $RErr_s$ is insensitive to A, and the reconstruction bias increases linearly with A. These results suggest that the spatial and mesoscale variability weaken the sensitivity of the reconstruction bias to the magnitude of the seasonal cycle and causes $RErr_s$ to decrease with A.

In contrast, $RErr_s^2$ increases with the strength of mesoscale variability B (Figure 2c), and the sensitivity is strongest at long length scales. This can be explained by the aliasing of the mesoscale signal to these length scales. For short and moderate length scales ($L_n < 5000$ km), $RErr_a$ is nearly insensitive to the strength of the seasonal cycle and mesoscale variability (not shown). The $RErr_a$ at long scales, in contrast, increases in the presence of time dependence, with the strongest sensitivity to B, but remains small.

In summary, RErr depends strongly on the spacing between floats as long as the dominant length scale in the system is not fully resolved. A stronger seasonal cycle is associated with improved skill in reconstructing that signal. Mesoscale variability acts to increase RErr, and the effects are especially large when the magnitude of this variability is large. The effect of float movement is a combination of the increase in spatial
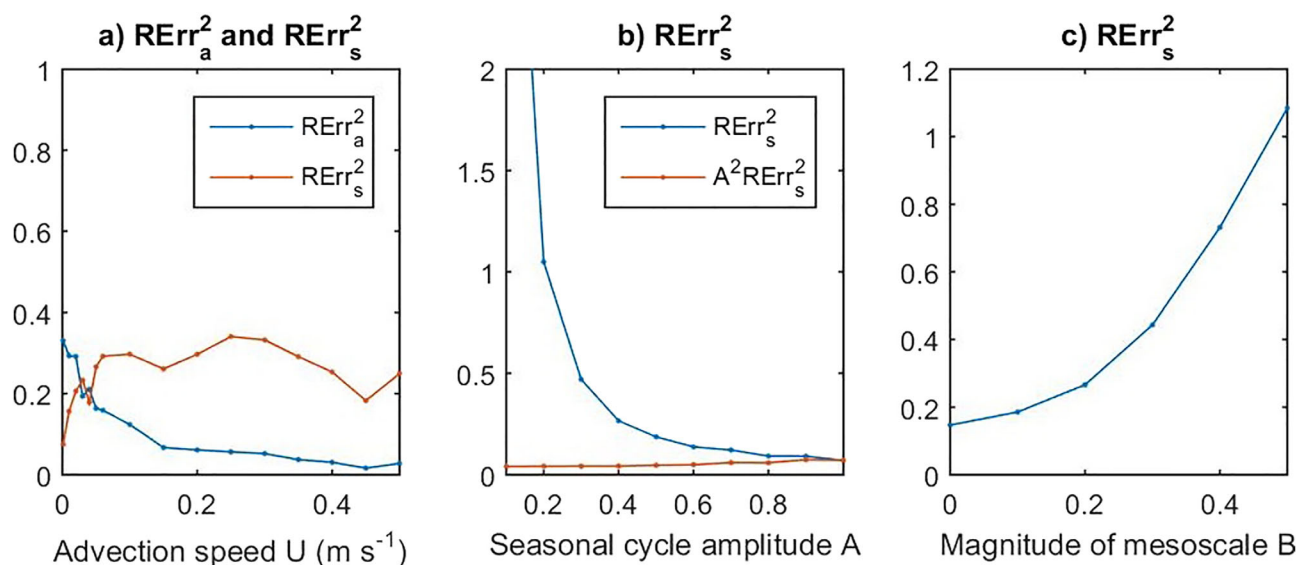
Figure 2. Sensitivity of the reconstruction skill to the main parameters in the idealized OSSE with a nominal array resolution of 670 km and $L/n = 4000$ km. (a) Dependence of $RErr_a^2$ and $RErr_s^2$ on the advection speed (U) for $A = 0.4$ and $B = 0.2$. (b) Dependence of $RErr_s^2$ on the magnitude of the seasonal cycle (A) for $U = 0.05$ m s^{-1} and $B = 0.2$; also shown is $A^2 RErr_s^2$. (c) Dependence of $RErr_s$ on the magnitude of mesoscale variability (B) for $U = 0.05$ m s^{-1} and $A = 0.4$.

sampling coverage, which leads to a decrease in the RErr for the annual mean, and the distortion of the seasonal cycle, which for small values of U leads to an increase in the RErr for the monthly climatology.

3. Full OSSEs: Models and Methods of Analysis

3.1. Simulated Biogeochemical Fields

The sampled fields, namely O_2 and DIC, are taken from a CM2.6 coupled climate simulation. CM2.6 is a coupled climate model first introduced by *Delworth et al.* [2012] and further analyzed by *Griffies et al.* [2015]. The model uses an atmospheric component of roughly 50 km horizontal resolution as well as sea ice and land model components. The oceanic component has a grid spacing of 0.1° (corresponding to a grid size of 5.5 km at 60°S) and has 50 levels in the vertical. The horizontal resolution is thus sufficiently high to simulate a rich mesoscale eddy field in the Southern Ocean [*Delworth et al.*, 2012, *Griffies et al.*, 2015]. CM2.6 is coupled to a biogeochemical model miniBLING [*Galbraith et al.*, 2015] which simulates DIC and O_2 as prognostic tracers. CM2.6 was run for 200 years under 1860 "preindustrial" atmospheric radiation based on a constant globally averaged CO_2 mixing ratio of 286 parts per million by volume (ppmv). A brief evaluation of the Southern Ocean state of the last 20 years of the CM2.6 preindustrial simulation can be found in *Dufour et al.* [2015].

A comparison of mean surface DIC and O_2 concentrations between observation-derived climatologies and the CM2.6 simulation shows an overall good agreement [see *Dufour et al.*, 2015, Figure 2]. Except along Antarctic coasts, modeled DIC concentrations were found to be higher than those from observations south of 40°S, with modeled O_2 concentrations showing the opposite bias. The major reason for those biases is likely to be an overexpression of the iron limitation in the modeled Southern Ocean [*Galbraith et al.*, 2015].

We first provide a brief description of the spatial and temporal variability of the model-simulated fields in the Southern Ocean, which will assist in interpreting RErr. For the analysis, we chose the surface values, because of their high spatiotemporal variability and relevance to air-sea fluxes, and the inventories in the top 2000 m, because of their importance in upper ocean budgets. Surface O_2 concentrations tend to decline equatorward, with the highest concentrations found poleward of the Subantarctic Front (SAF) and the strongest gradients located near the SAF (Figure 3a). In contrast, the largest values in the 2000 m inventories, reported as a vertical average over the top 2000 m, are found north of the SAF, roughly coinciding with the deep mixed layers south of Australia and in the South Pacific and South Indian basins (Figure 3b). In the South Atlantic, the inventories are more spatially uniform than the surface O_2 concentrations. The standard
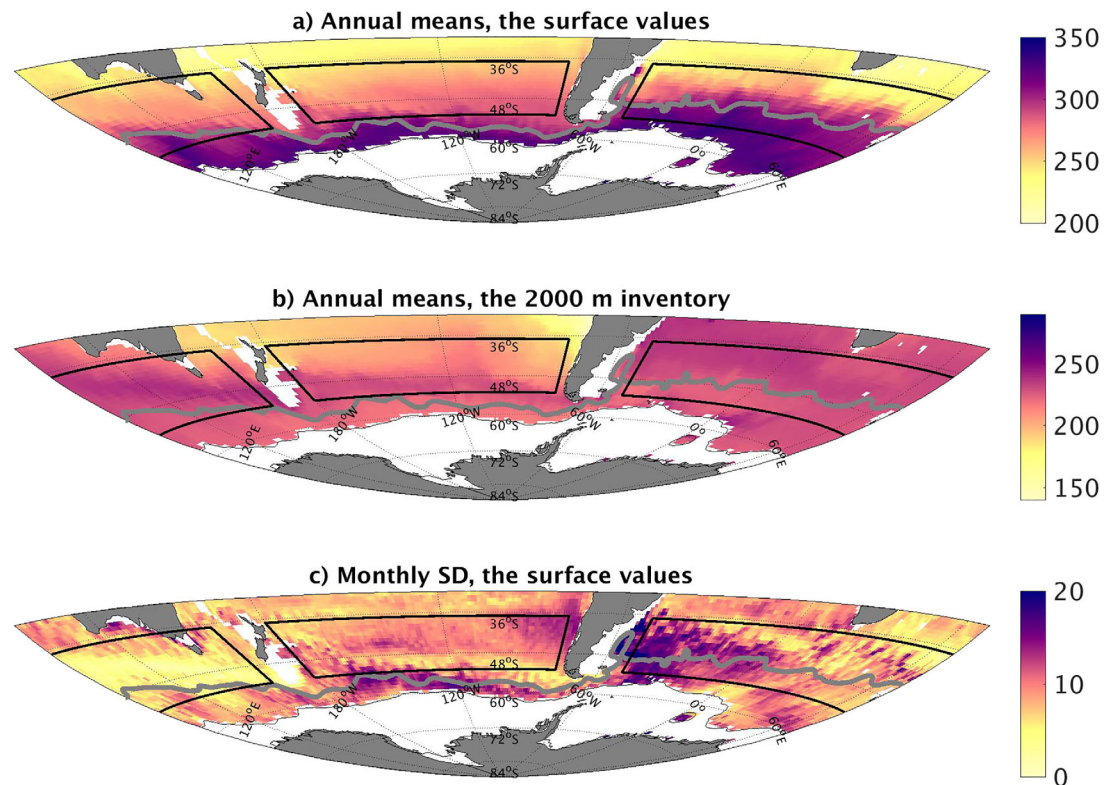
Figure 3. O$_2$ climatology from 5 years of CM2.6 simulations, reported on the 1° × 1° grid. (a) Annual-mean values at the surface; (b) annual-mean values in the inventories (average over the top 2000 m); and (c) standard deviation of monthly climatology of the surface values. Units are μmol kg^{-1}. Ice-covered (with the ice fraction > 0.25) areas and areas shallower than 2000 m are masked. For reference, the position of the SAF in the real ocean [*Orsi et al.*, 1995] (http://gcmd.nasa.gov/records/AADC_southern_ocean_fronts.html) is shown by the gray contour line. Two box regions used for the analysis are also shown by the black lines.

deviation (SD) of the monthly mean surface values is large in the Southeast (SE) Pacific, in the vicinity of the SAF and in the Western South Atlantic. In contrast, the SD is small in the Indian and south of Australia where the mixed layer is deep in winter.

Our idealized OSSEs demonstrated that the magnitude of the seasonal cycle (parameter A) and mesoscale variability (parameter B) are two important parameters that influence the reconstruction skill for the seasonal cycle. We now attempt to estimate these parameters from the model-simulated O$_2$. For a variable *F*, these parameters are estimated from the spatial variance $VAR(F) = \left\{ (F - \{F\})^2 \right\}$, where {...} stands for the spatial average, calculated in two regions depicted in Figure 3. Nondimensional parameters *A* and *B* can then be estimated as

$$ A \approx \left\{ \frac{2 \langle VAR(O_2 - \langle O_2 \rangle) \rangle}{VAR(\langle O_2 \rangle)} \right\}^{\frac{1}{2}}, \quad B \approx A \left\{ \frac{M(O_2)}{\langle (\{O_2\} - \langle \{O_2\} \rangle)^2 \rangle} \right\}^{\frac{1}{2}} \tag{5} $$

where the angle brackets denote annual-mean values and $M(O_2)$ stands for the area-averaged mesoscale variance in O$_2$. Mesoscale anomalies are defined as deviations of the 5 day fields on the original 1/10°grid from the monthly means on the 1° grid. Note that if the various terms in equation (5) are calculated for the idealized fields in section 2, then $\langle VAR(O_2 - \langle O_2 \rangle) \rangle = \frac{1}{4} A^2 C_n^2$, $VAR(\langle O_2 \rangle) = \frac{1}{2} C_n^2$, and $\langle (\{O_2\} - \langle \{O_2\} \rangle)^2 \rangle = \frac{1}{2} A^2$. For the surface O$_2$, we get $A = 0.4$ (0.3) for the Pacific (Indo-Atlantic) regions and the parameter *B* is 0.2. Note that, according to our idealized model, these numbers suggest lower reconstruction skill in the Indo-Atlantic region.

For DIC, the annual-mean distribution of the 2000 m inventories resembles the surface distribution (Figure 4), although the meridional gradients are sharper in the Atlantic and weaker in the Indo-Pacific sectors. Similar to O$_2$, the SD of the monthly mean surface values has strong maxima in the vicinity of SAF in
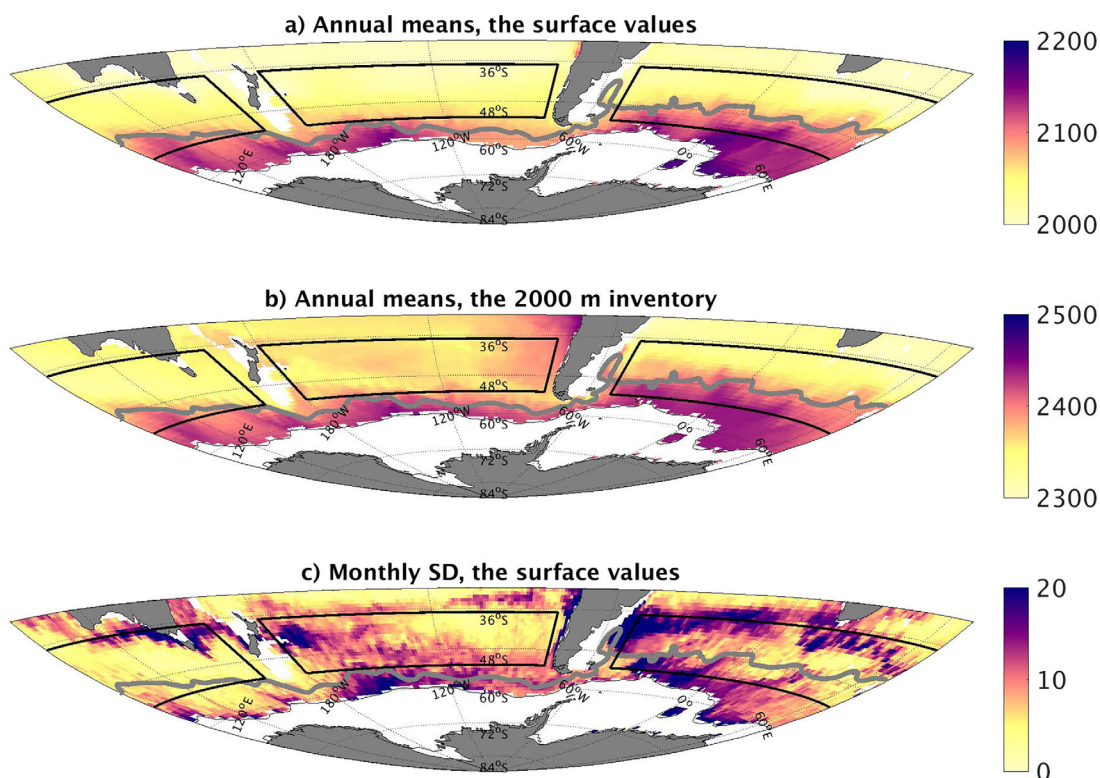
Figure 4. DIC climatology from 5 years of CM2.6 simulations, reported on the 1° × 1° grid. (a) Annual-mean values at the surface; (b) annual-mean values in the inventories (average over the top 2000 m); and (c) standard deviation of monthly climatology of the surface values. Units are μmol kg^{-1}. Ice-covered (with the ice fraction > 0.25) areas and areas shallower than 2000 m are masked. For reference, the position of the SAF in the real ocean (http://gcmd.nasa.gov/records/AADC_southern_ocean_fronts.html) is shown by the gray contour line. Two box regions used for the analysis are also shown by the black lines.

the Pacific basin and in the Southwestern (SW) Atlantic. The main difference with the O_2 distribution is found north of the SAF in the Southeastern (SE) Pacific, where the annual cycle in DIC is weak. Instead, the annual cycle is strong just east of New Zealand. Our estimates result in $B = 0.2$ (0.3) for the Pacific (Indo-Atlantic) regions, and $A = 0.3$ for surface values in both regions. Note that the ratio A/B for DIC is 1.5 (1.0) Pacific (Indo-Atlantic) regions and is lower than the same ratio for O_2 (2.0 and 1.5, respectively), which hints at lower reconstruction skill for DIC.

3.2. Location of Profiles

Conclusions from OSSEs can be very sensitive to where and when the profiles are taken. The trajectories of SOCCOM floats are largely unknown, both because most of the deployment sites are not yet finalized and because model projections of ocean currents can have biases. In this study, we account for sensitivity of the conclusions to profile locations by using a wide range of trajectories and analyze an ensemble of model-simulated and actual Argo trajectories for years 2010–2014. The real Argo float profile locations and times were downloaded from the Argo Global Data Assimilation Centre (http://www.usgodae.org/ftp/outgoing/argo). The model-simulated Argo trajectories were taken from separate OSSEs designed for the global Argo array that are currently in progress. These global OSSEs use velocities from a global data-assimilating HYCOM climatological simulation with 1/12° horizontal resolution and 32 vertical layers (simulation GLBa0.08). This simulation without Argo floats has already been carried out and the daily horizontal velocities that we use here for calculation of Argo trajectories were downloaded from the HYCOM data portal (www.hycom.org). In a manner that closely resembles the real Argo array, the simulated floats were advected at the depth of 1000 m for 9 days, followed by a 6 h ascent during which a profile over 2000 m is taken, 12 h of surface advection (note that this design is relevant to most Argo floats, whereas SOCCOM floats typically spend less than 1 h at the surface), and a 6 h descent to the 1000 m depth. Their trajectories were initialized at the actual Argo deployment sites. During their ascent (descent), the floats were advected using velocities that are depth averaged over the upper 2000 m (1000 m). We did not use CM2.6 velocities

because daily velocities from CM2.6 simulations are only available at the surface. As a result, tracer fields and 1000 m float trajectories are not necessarily consistent, which introduces some uncertainty in our conclusions. This additional uncertainty, which will depend on how strongly the 1000 m trajectories are correlated with the field being reconstructed, is not accounted for explicitly here.

The analysis is based on an ensemble of N five-year-long float trajectories. If the actual Argo trajectories did not last until the end of 2014, they were artificially extended using Argo trajectories that began after 2010 and ended after 31 December 2014. Our control simulation has $N = 150$; sensitivity experiments that varied the number of floats were also carried out. These N trajectories were randomly selected from a large group of more than 400 Argo trajectories. Five sets of N HYCOM-generated and five sets of N actual Argo trajectories were used for the analysis. The RErr was calculated for each of these 10 sets, and we analyze both the mean and SD of the resulting ensemble of RErr.

3.3. Reconstruction Errors

The reconstruction of O_2 and DIC was carried out using a multiscale objective analysis technique [*Gray and Riser*, 2015]. This method uses an iterative generalized least squares fitting procedure combined with a standard objective mapping algorithm to map large-scale and small-scale fields, respectively. The large-scale signal is fit to a set of spherical radial basis functions, and the analysis is iterated to find optimal spatiotemporal scales to use in the objective mapping procedure. Accordingly, the primary advantage of this technique is that those scales are optimized based on the data instead of specified in an ad hoc manner.

For the full OSSEs, we again use the reconstruction error as the metric of reconstruction skill, defined here as a weighted difference (bias) between the reconstructed ($F^{(reconst)}$) and actual model ($F^{(model)}$) fields. The weighting establishes the significance of this difference relative to the signal we are trying to recover from the synthetic observations. For the annual mean, the mean bias is weighted by a measure of spatial variability on long spatial scales:

$$RErr_a = \left(\langle F^{(reconst)} \rangle - \langle F^{(model)} \rangle \right) |\nabla \langle F^{(model)} \rangle \cdot \boldsymbol{L}|^{-1} \tag{6}$$

where ∇ is the horizontal gradient, $\boldsymbol{L}$ is the vector length scale, taken to be (800 and 300 km) and the angle brackets denote the average over 12 monthly means. For the definition of the spatial variability on scales $\boldsymbol{L}$, $F^{(model)}$ in the denominator of (6) is spatially smoothed by a running 2-D mean with length scale $\boldsymbol{L}$. This scale roughly corresponds to the average spacing between floats, but it was verified that the conclusions are qualitatively insensitive to the choice of the ratio between the zonal and meridional scales.

For the seasonal cycle, the RErr is defined as the SD of the monthly biases weighted by the SD of the monthly values:

$$RErr_s = SD \left(F^{(reconst)} - F^{(model)} \right) \left\{ SD \left(F^{(model)} \right) \right\}^{-1} \tag{7}$$

No spatial smoothing is used in (7). These definitions are used in the rest of this study, with the exception of the analysis of the sensitivity to the length scale in section 4.2. In this study, we will analyze the square of (6) and (7), which can be interpreted as the normalized mean squared reconstruction bias. In the following analysis, we interpret $RErr^2 > 0.5$, that is, the mean squared bias is greater than half the variance in the signal, as an indicator of unreliable reconstruction, and $RErr^2 < 0.5$ as an indicator of good reconstruction skill. This choice of the threshold for good/low reconstruction skill is, of course, not unique, and should be made according to the goals of each individual study. Note also that the weighted RErr in (6)–(7) can be larger than 1.0, which indicates particularly poor reconstruction skill in places where the sampled profiles are too sparse to produce a reliable estimate.

4. Full OSSEs: Results

4.1. RErr in the Control Simulation With 150 Floats

The analysis here is based on both the mean and SD of the 10-member ensembles of $RErr_a^2$ and $RErr_s^2$ (section 3.2). Overall, ensemble-mean values show some regions with persistently large reconstruction errors, such as the vicinity of the ice edge where the spatial sampling density for the Argo array is very low (Figure 5). Note that because spatial sampling coverage of Argo floats is still very poor in seasonally
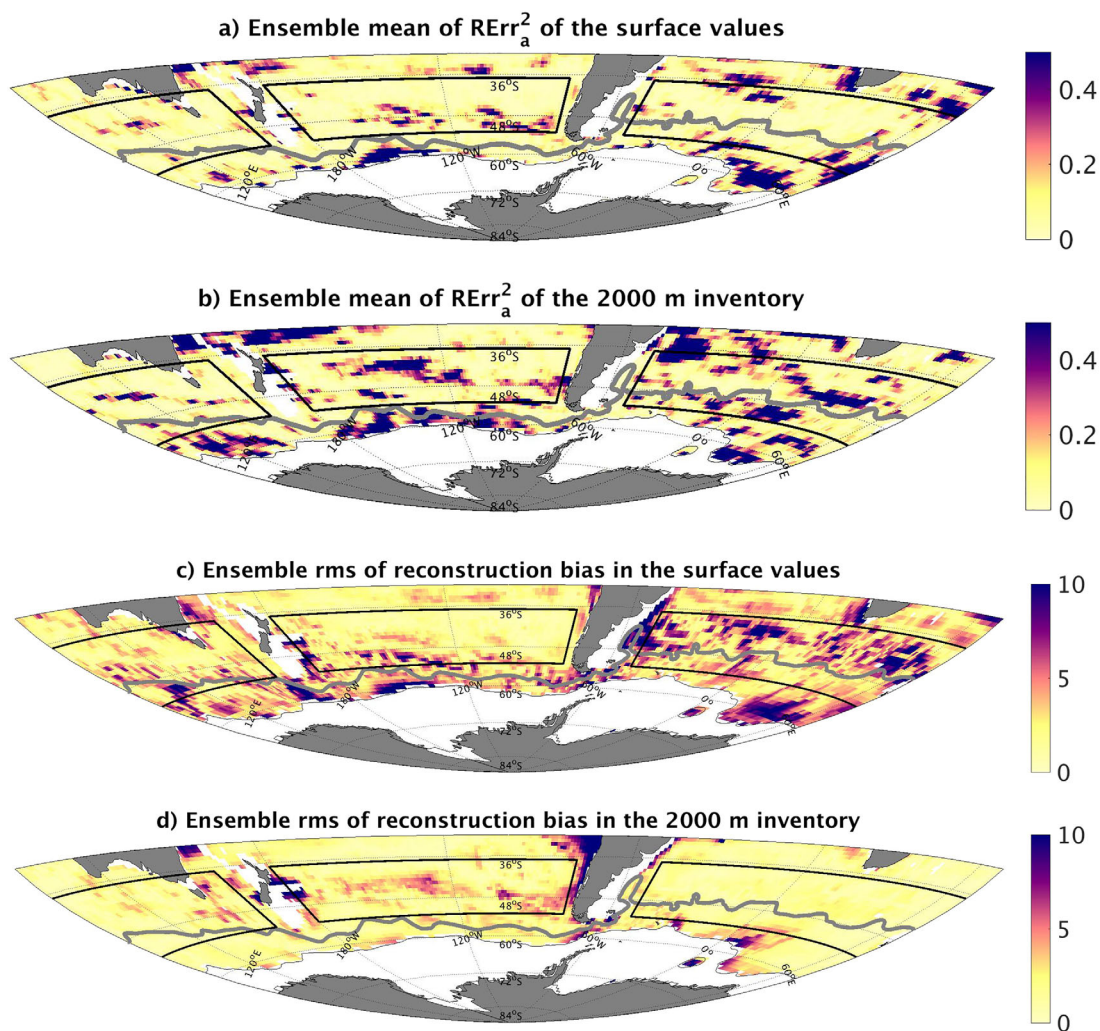
Figure 5. Reconstruction skill of the annual-mean O_2 for 150 trajectories, based on an ensemble of 10 simulations. Figures show (a, b) ensemble-mean $RErr_a^2$ and (c, d) the ensemble rms of the reconstruction bias (numerator in equation (6)), for both surface values (Figures 5a and 5c) and 2000 m inventories (Figures 5b and 5d). Units in Figures 5c and 5d are μmol kg^{-1}. Ice-covered (with the ice fraction > 0.25) areas and areas shallower than 2000 m are masked. For reference, the position of the SAF in the real ocean is shown by the gray contour line. Two box regions used for the analysis are also shown by the black lines.

ice-covered areas, these regions are excluded from the current analysis. Ensemble-mean $RErr_a^2$ for surface O_2 also exhibits local maxima (exceeding 0.5) in the Pacific sector of the ACC (near 48°S) and the southern part of the Atlantic subtropical gyre (Figure 5a). Apart from these two regions, $RErr_a^2$ is generally very low at the surface, especially in the South Pacific (north of 48°S). In this region, the absolute bias (numerator in equation (6)) is low (Figure 5c), and the spatial variability in the model fields (denominator in equation (6); Figure 6a) is high, which results in small $RErr_a$ and high reconstruction skill for the spatial variability. Area-averaged RMS values are computed for the $RErr^2$ in two geographical regions, the South Pacific and the Atlantic-Indian sectors of the Southern Ocean (shown by black boxes in Figures 3–8). The area averages for these regions are dominated by a few small areas with large RErr. To remove the effect of those areas, we determine the fraction of each region that had a reliable reconstruction ($RErr^2 < 0.5$) and then average the RMS values from only those areas. In both regions, the reconstruction skill is good ($RErr_a^2 < 0.5$) in 97% of the area, where the area-averaged RMS of $RErr_a^2$ is found to be 0.05 (Table 1). The $RErr_a^2$ is larger in the 2000 m inventory than at the surface (Figure 5b), especially in the South Atlantic around 36°S, primarily due to the weak spatial variability (i.e., small gradients) in the subsurface layers (Figure 6b). Large $RErr_a$ in the inventories is also observed in the vicinity of the SAF and in the South Pacific around 40°S.

The idealized studies in section 2 demonstrated that for a given number of floats, the reconstruction skill is affected by the magnitude of the seasonal cycle, mesoscale variability, and float advection speed. In
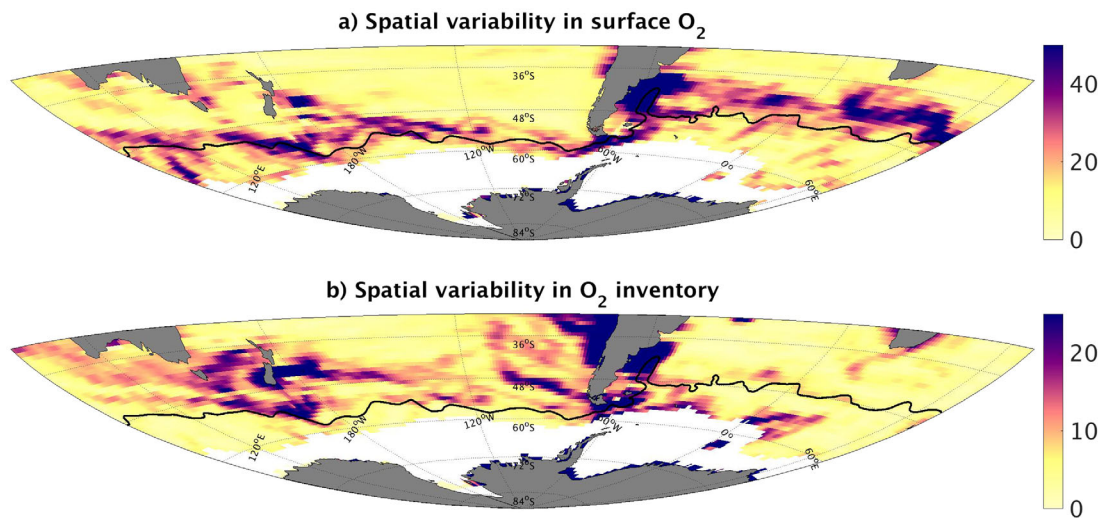
a) Spatial variability in surface O$_2$

b) Spatial variability in O$_2$ inventory

Figure 6. Measure of spatial variability (denominator in equation (6)) for (a) surface O$_2$ and (b) 2000 m O$_2$ inventory. Units are μmol kg^{-1}. For reference, the position of the SAF in the real ocean is shown by the gray contour line.

addition, spatial sampling density for the full OSSEs—the total number of profiles within a unit area—will be uneven. Geographical distribution of these properties is shown in Figures 3c and 8a–8c. According to the analysis in section 2, RErr$_a$ can be expected to decrease in the regions where the profiling floats are moving fast, increase for long length scales if mesoscale variability is high, and remain relatively insensitive to the seasonal cycle. Fast float advection in the SW Atlantic and Agulhas region (Figure 8b) indeed
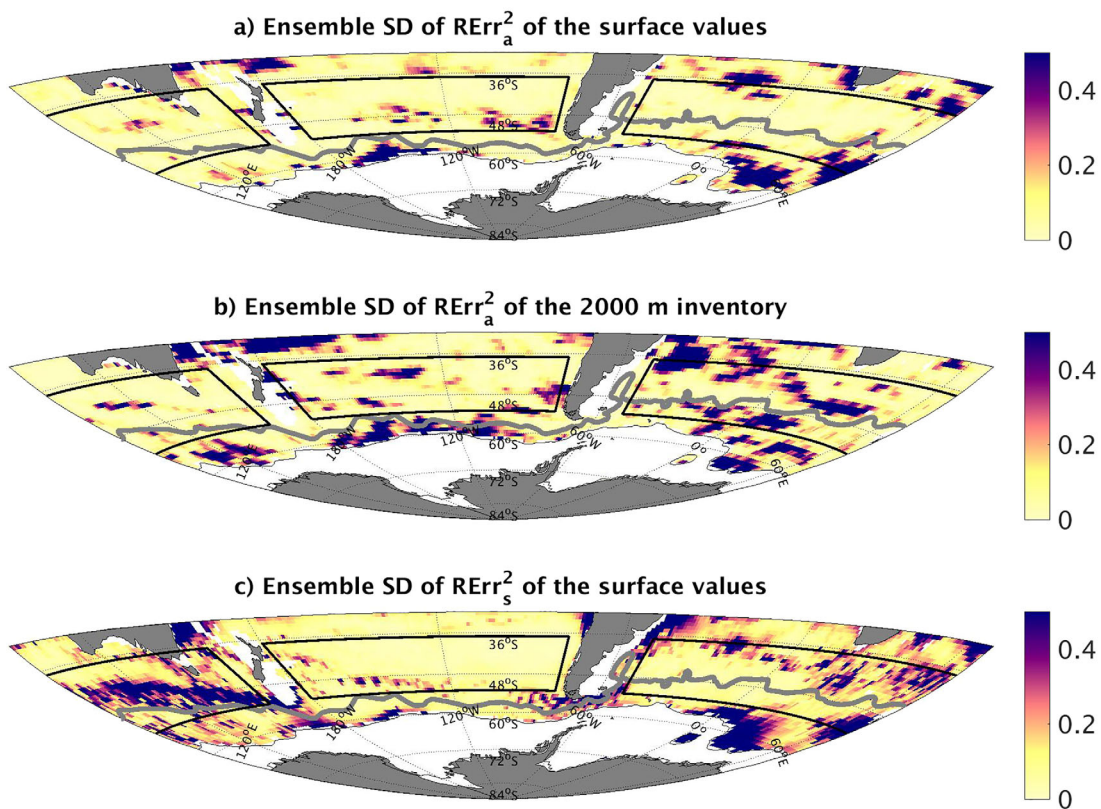
a) Ensemble SD of RErr$_a^2$ of the surface values

b) Ensemble SD of RErr$_a^2$ of the 2000 m inventory

c) Ensemble SD of RErr$_s^2$ of the surface values

Figure 7. Ensemble standard deviation for (a) RErr$_a^2$ in the surface values; (b) RErr$_a^2$ in the inventories; and (c) RErr$_s^2$ in the inventories. Ice-covered (with the ice fraction > 0.25) areas and areas shallower than 2000 m are masked. For reference, the position of the SAF in the real ocean is shown by the gray contour line. Two box regions used for the analysis are also shown by the black lines.
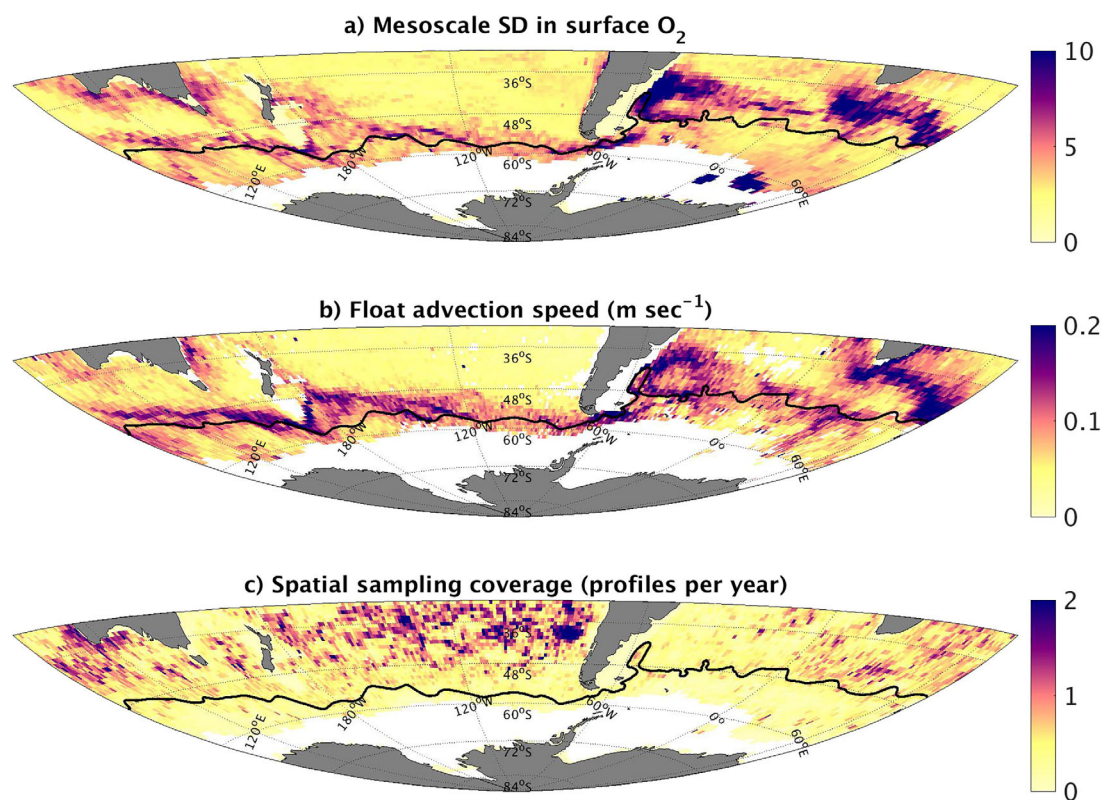
Figure 8. Factors affecting the reconstruction skill. (a) Mesoscale variability in the surface O_2, estimated by the mean square of deviations from the monthly mean. (b) Float advection speed, estimated from the profile locations. (c) Spatial sampling coverage. Ice-covered (with the ice fraction > 0.25) areas and areas shallower than 2000 m are masked. For reference, the position of the SAF in the real ocean is shown by the black contour line.

coincides with low $RErr_a$, despite relatively low spatial sampling density and high mesoscale variability. In contrast, $RErr_a$ is high in the vicinity of the SAF in the Pacific sector, where high mesoscale variability degrades the reconstruction skill despite fast float movement. Finally, low spatial sampling coverage (Figure 8c) explains large reconstruction errors in the South Atlantic.

$RErr_s$ for O_2 is on average higher than $RErr_a$ (Table 1) and indicates that several regions have poor reconstruction skill. For example, the surface $RErr_s$ is very large (>1) south of Australia (Figure 9a). The monthly bias (bracketed expression in the numerator in equation (7), Figure 9b) is large in this region of strong meridional gradients, but the seasonal cycle is weak (Figure 3c), which results in a large $RErr_s$. High mesoscale variance (Figure 8a) is consistent with large $RErr_s$ near the SAF (south of Australia) and in the Agulhas region and Indian Ocean. In the rest of the domain, the $RErr_s$ is significantly smaller, suggesting high reconstruction skill for the seasonal cycle. For example, the $RErr_s$ is low in the vicinity of the Atlantic and Pacific SAF and in the SW Atlantic and SE Pacific, which is primarily explained by the strong seasonal cycle in these regions (Figure 3c). Near the SAF and in the SW Atlantic, low spatial sampling density and high mesoscale variance do not degrade the reconstruction skill. Overall, $RErr_s^2 < 0.5$ in 94% (63%) of the Pacific (Atlantic-Indian) regions (Table 1). The $RErr_s^2$ in the 2000 m inventory is larger than 0.5 in most of the domain, which is explained by the weak seasonal cycle ($A = 0.1$–0.2 according to equations (5)). Hence, the reconstruction of the seasonal cycle in the inventories is not discussed in the rest of this study.

Ensemble SDs of $RErr_a^2$ and $RErr_s^2$ in O_2 serve as a measure of the sensitivity of

Table 1. Reconstruction Skill for O_2 (First Row) and DIC (Second Row) for the Control Simulation ($N = 150$)[a]

	$RErr_a^2$ Surface	$RErr_s^2$ Surface	$RErr_a^2$ Inventory
Pacific: O_2	0.05 (0.97)	0.12 (0.94)	0.08 (0.93)
Pacific: DIC	0.1 (0.92)	0.23 (0.81)	0.08 (0.87)
Atlantic-Indian: O_2	0.05 (0.97)	0.21 (0.63)	0.07 (0.94)
Atlantic-Indian: DIC	0.05 (0.98)	0.27 (0.41)	0.045 (0.97)

[a]Reported is the area-averaged $RErr^2$ in the two geographical regions shown in Figures 3–8. The averaging is carried out only over the regions where $RErr^2 < 0.5$. The ratio of the area with high reconstruction skill to the total area is shown in parentheses.
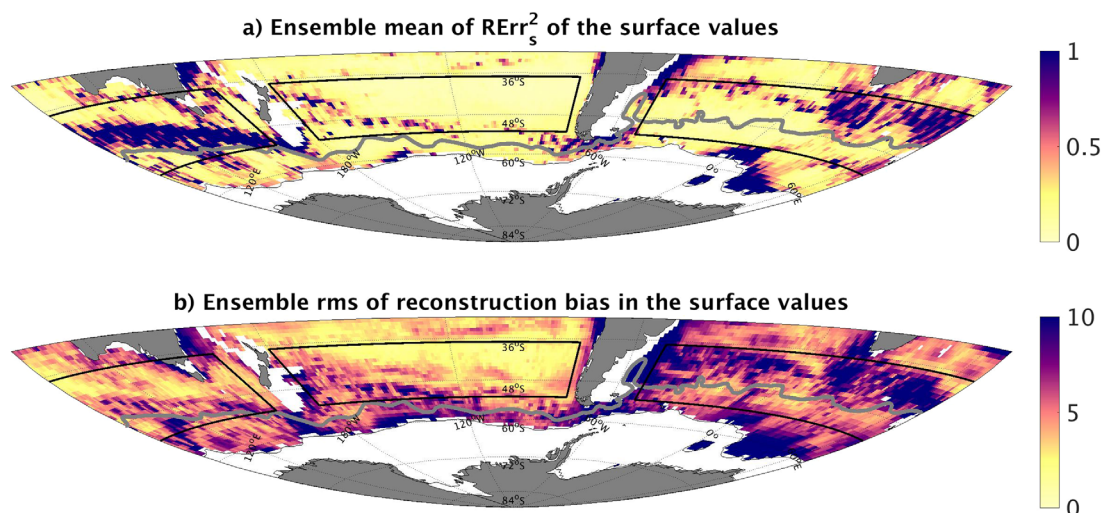
a) Ensemble mean of $RErr_s^2$ of the surface values

b) Ensemble rms of reconstruction bias in the surface values

Figure 9. Reconstruction skill of the seasonal cycle in O_2 for 150 trajectories, based on an ensemble of 10 simulations. Figures show (a) ensemble mean of $RErr_s^2$ and the ensemble rms of the reconstruction bias (units are μmol kg^{-1}). Ice-covered (with the ice fraction > 0.25) areas and areas shallower than 2000 m are masked. For reference, the position of the SAF in the real ocean is shown by the gray contour line. Two box regions used for the analysis are also shown by the black lines.

the RErr to specific float trajectories and, therefore, of the uncertainty in our estimates of the reconstruction skill. SD values are lower than 0.5 in most of the domain and are particularly small north of the ACC and south of 36°S (Figures 7c and 7d), which suggests high confidence in the OSSE-based predictions of the reconstruction skill in this region. The SDs are larger in the ACC and the South Atlantic and South Indian. Large SD values tend to coincide with low spatial sampling coverage, which is not surprising since the RErr is expected to be most sensitive to the profile locations in places where the profiles are sparse. Combined with relatively high values of the ensemble-mean $RErr^2$, these results therefore suggest the need for denser data sampling in these regions.

The reconstruction skill for DIC has several significant differences compared to that for O_2. The magnitude of the $RErr_a^2$ for surface DIC is larger than for O_2 in the Pacific sector (Table 1), consistent with a more uniform spatial distribution of the former quantity (Figure 10a), but is similar to O_2 in the Atlantic-Indian sector. The opposite is true for the inventories, with the $RErr_a^2$ for DIC smaller than the error for O_2 in the Atlantic-Indian sector and similar in the Pacific. The $RErr_s^2$ is larger for DIC than for O_2 everywhere in the domain (Table 1 and Figures 10c and 10d). At the surface, the largest differences are observed in the reconstruction of the seasonal cycle in the SE Pacific, due to the weak seasonal cycle in this region.

4.2. Sensitivity of RErr in O_2 to Length Scales

In this section, we examine how the reconstruction skill depends on the length scales in the reconstructed O_2 field. For this analysis, both of the boxed regions shown in Figures 3–8 were further divided into several nonoverlapping square subregions where the reconstruction error is defined by

$$\widetilde{RErr}_a^{\,2} = \left\{ \left[\langle O_2^{(reconst)} \rangle - \langle O_2^{(model)} \rangle \right]^2 \right\} \left\{ \left(\left[\langle O_2^{(model)} \rangle \right] - \left\{ \left[\langle O_2^{(model)} \rangle \right] \right\} \right)^2 \right\}^{-1} \tag{8}$$

$$\widetilde{RErr}_s^{\,2} = \left\{ \left\langle \left[O_2^{(reconst)} - O_2^{(model)} - \langle O_2^{(reconst)} - O_2^{(model)} \rangle \right]^2 \right\rangle \right\}$$

$$\left\{ \left\langle \left[O_2^{(model)} - \langle O_2^{(model)} \rangle \right]^2 \right\rangle \right\}^{-1} \tag{9}$$

The above equations use the following notations: [. . .] denotes the spatial smoothing using a two-dimensional L by L running-mean filter; {. . .}. area averaging; and <. . .> stands for the average over 12 monthly values. The spatial smoothing and averaging are done for all values including regions with large reconstruction bias. As in our standard definition, small (<0.5) values of $RErr^2$ indicate good reconstruction skill.
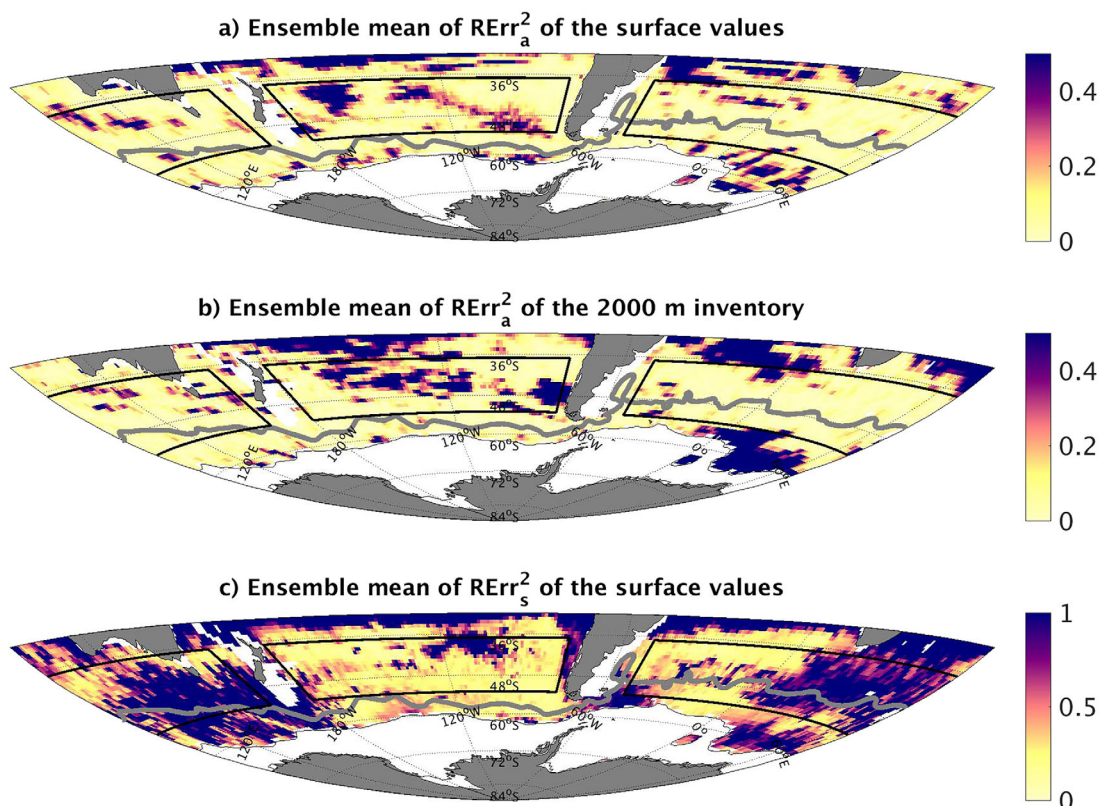
Figure 10. Reconstruction skill of the annual mean and seasonal cycle for DIC for 150 trajectories, based on an ensemble of 10 simulations. (a) $RErr_a^2$ for the surface values; (b) $RErr_a^2$ for the 2000 m inventories; and (c) $RErr_s^2$ for the surface values. Ice-covered (with the ice fraction > 0.25) areas and areas shallower than 2000 m are masked. For reference, the position of the SAF in the real ocean is shown by the gray contour line. Two box regions used for the analysis are also shown by the black lines.

Figure 11 shows the ensemble mean of $\widetilde{RErr_a}^2$ and $\widetilde{RErr_s}^2$. Results show that $\widetilde{RErr_a}^2$ and $\widetilde{RErr_s}^2 < 0.5$ for all fields. Overall, the weighted biases decrease with increasing L, since the removal of short length scales increases the reconstruction skill. The bias for the annual-mean inventories seems to reach a near constant value for $L > 1000$ km (Figure 11b), but for other quantities, the bias continues to decrease for longer length scales. For example, for the surface values, the bias declines by more than a factor of 5 between $L = 100$ km and $L = 1800$ km. Note that we cannot extend this analysis to longer length scales because of the geometrical limitations of the smoothing operator.

As was demonstrated in section 2, the shortest length scale that can be accurately reconstructed—the "effective resolution" of the array—is several times longer than the average spacing between floats. The average spacing is not easy to determine in a full OSSE, but dividing the area of the ocean between 60°S and 30°S at 2000 m depth by the number of floats (150) and taking the square root gives an estimated float spacing of approximately 750 km. The results of the idealized OSSE, which found that length scales greater than 5 times the float spacing are well resolved, would then suggest that in this case the RErr should asymptote for $L > 3750$ km. However, the average spacing between floats is not always an accurate predictor of the effective resolution of the array due to the complexity of the domain, float movement, and variability in the sampled field. In addition, the reconstruction in the full OSSEs is based on 5 years of synthetic measurements, whereas the idealized study was based on 1 year of idealized data, and it is unclear how the interannual variability affects the results.

4.3. Sensitivity of RErr in O₂ to the Number of Floats

To study the dependence of the reconstruction skill on the number of floats, we carried out a set of 10-member ensembles for $N = 50, 100, 150, 200$, and 300. Since the spatial scales used in the objective mapping procedure are determined from the data itself, they are optimized for each reconstruction, and not adjusted in an ad hoc manner. The reconstruction skill was quantified by the $RErr_a^2$ and $RErr_s^2$, area averaged
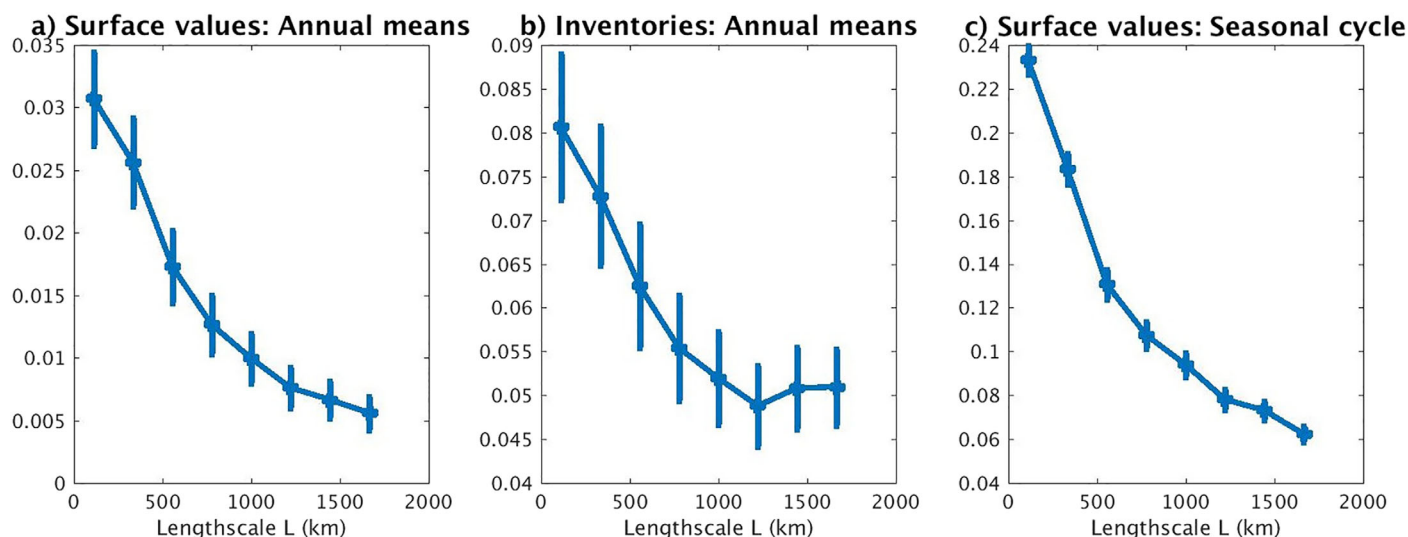
Figure 11. Effective resolution of the array of 150 floats. The absolute reconstruction errors are spatially smoothed with a running-mean L by L filter, weighted by a measure of spatio-temporal variability, squared and area averaged; see section 4.2 for details. (a) Annual-mean surface values; (b) annual-mean inventories; and (c) monthly surface values. Shown are the ensemble-mean values together with uncertainty range.

within the South Pacific and South Atlantic-Indian regions shown in Figures 3–8, excluding areas with poor reconstruction skill ($RErr^2 > 0.5$).

The results given in Figure 12 show that in general, the $RErr_a$ is more sensitive to N than the $RErr_s$. This finding, which is consistent with the idealized OSSEs (Figure 1b), is explained by the fact that $RErr_a$ is mainly a function of the spacing between floats, whereas $RErr_s$ is also strongly affected by the sampling frequency. All RErr decrease substantially with increasing N. In general, the RErr exhibits a moderate decline when N is increased from 150 to 300 but decreases more rapidly when N increases from 50 to 150. To describe this behavior, we define a parameter that quantifies the change in the slope of the $RErr^2(N)$ (Figure 12) between $N = 50$ to $N = 150$ and $N = 150$ to $N = 300$:

$$\alpha = \left(\frac{RErr^2(N=50) - RErr^2(N=150)}{100} \right) \left\{ \frac{RErr^2(N=150) - RErr^2(N=300)}{150} \right\}^{-1} \qquad (10)$$

where RErr are defined by either (6) or (7). This parameter is unity if RErr decreases linearly with N and is >1 if the sensitivity to N weakens with larger N.

For both the geographical regions examined here, α is indeed >1 for both $RErr_a$ and $RErr_s$ (Table 2). The largest values are found for $RErr_a$ at the Pacific surface and $RErr_s$ at the Atlantic-Indian, although even these values are <2.2. Overall, these results suggest that while substantial gains in reconstruction skill are realized when the number of floats increases from 50 to 150, further increasing the number of floats from 150 to 300 gives a comparatively small improvement. Our idealized OSSEs demonstrate that such behavior can be expected for fields dominated by relatively long length scales (Figures 1c and 1d), because they can be resolved by fewer floats and further increasing the number of floats does not significantly improve the reconstruction skill.

For the annual-mean fields, more than 90% of the regions have $RErr_a^2 < 0.5$ for $N > 100$. Bringing the RErr to zero everywhere in the domain would, however, require dense spatial coverage in several "problematic" (e.g., parts of ACC) spots. Notably, $RErr_s$ remains large in the South Indian Ocean and Agulhas region even for $N = 300$. Note also that none of the fields exhibit a clear asymptotic behavior for these values of N. Dramatically increasing the number of floats would undoubtedly bring the RErr closer to zero but likely is not achievable for practical reasons. An optimized distribution of floats, with more floats in these problematic spots, would also produce smaller RErr.

Table 2. Parameter α; See Section 4.3 for the Definition[a]

	$RErr_a$ Surface	$RErr_s$ Surface	$RErr_a$ Inventory
Pacific	1.9	1.5	1.5
Atlantic-Indian	1.5	2.1	1.8

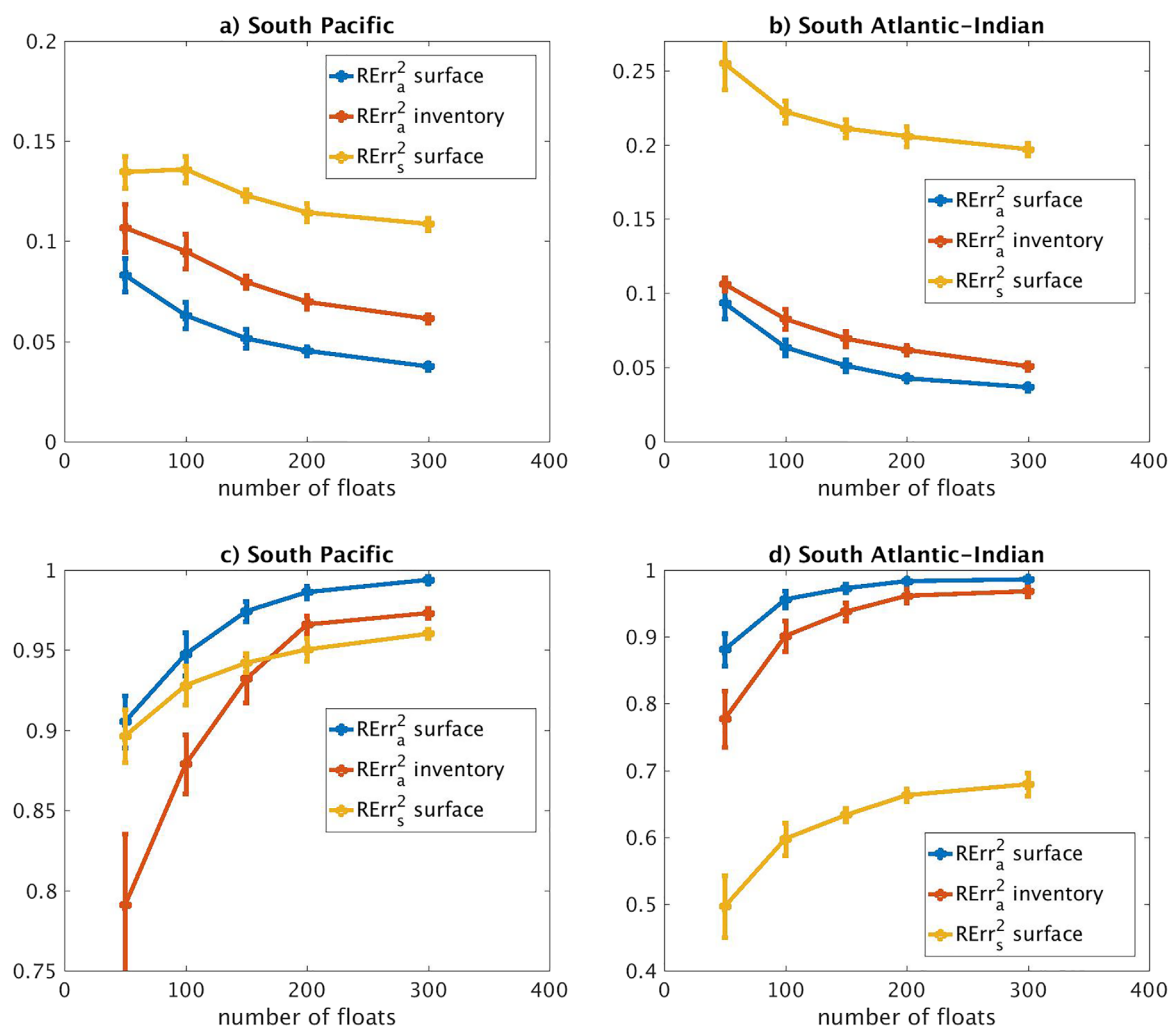[a]Values > 1 indicate decreasing sensitivity of RErr to N for $N > 150$.

Figure 12. Dependence of the reconstruction skill for O_2 on the number of floats. (top row) Ensemble-mean area-averaged $RErr^2$ with an uncertainty range; the averaging is carried only over the regions where $RErr^2 < 0.5$. (bottom row) Portion of the total region area where $RErr^2 < 0.5$. The geographical regions are shown by black lines in Figures 3–8.

5. Summary and Discussion

This study uses OSSEs to examine the reconstruction skill of biogeochemical variables in the Southern Ocean observed with SOCCOM profiling floats. Focusing on the reconstruction of a climatology, we address the reconstruction skill for the geographical distribution in both the annual-mean fields and the seasonal cycle. Two variables are considered by this study: O_2, which is directly measured by the SOCCOM array, and DIC, which is inferred from the SOCCOM measurements. The reconstruction skill is quantified by the reconstruction error (RErr), defined as the difference between the reconstructed and actual model-simulated fields (reconstruction bias) weighted by a local measure of the spatiotemporal variability (i.e., the signal that the objective mapping is intended to recover). Using RErr as our metric, we find that for an array of floats resembling the planned SOCCOM array, the reconstruction skill is good ($RErr^2 < 0.5$) over most of the domain for the annual mean at the surface and in the inventories, and for the seasonal cycle at the surface. Both the idealized and comprehensive OSSEs suggest the importance of the magnitude of the seasonal cycle and spatial tracer gradients, the speed of the float movement, the strength of mesoscale variability, and the number of floats. These factors explain a large part of the spatial variability in the reconstruction skill and can be used to predict the reconstruction skill of the actual SOCCOM array.

The square of RErr can be interpreted as the mean squared reconstruction bias normalized by the magnitude of the signal and thus as an uncertainty on a mapped climatology. This definition of RErr is consistent with the fact that the reconstruction bias is caused by a limited number of observations of a field that is

changing in time and space, and the bias is, therefore, expected to increase with variability. According to the idealized model, $RErr_s$ is not sensitive to the magnitude of the seasonal cycle for a tracer which is spatially uniform and has no mesoscale variability. In the presence of spatial variability and mesoscale "noise," however, $RErr_s$ decreases with the strength of the monthly variability. This result is further confirmed by the comprehensive OSSEs, which show that $RErr_s$ is low in regions where the seasonal cycle is strong. In simple terms, it is easier to reconstruct a strong signal.

The reconstruction skill also depends heavily on the spatial sampling density [e.g., *Kamenkovich et al.*, 2009], which is determined by the number of deployed floats N and by the float movement. Our idealized OSSE demonstrated that accurate recovery of a time-varying signal of a given length scale requires the average separation between floats data points to be approximately 1/5 of that length scale. However, once the length scale is resolved, further increases in N do not bring significant reduction in RErr. Full OSSEs indeed demonstrate that RErr tends to asymptote for $N > 150$ and, thus, a doubling of N from 150 to 300 appears unlikely to significantly improve reconstruction of the climatology of O_2. This conclusion is in close agreement with *Majkut et al*. [2014], who analyzed reconstruction of the air-sea CO_2 flux from measurements taken at randomly distributed fixed locations and concluded that 200 floats is sufficient to reconstruct the seasonal climatological CO_2 flux with minimal error. The agreement between our results and *Majkut et al*. [2014] suggests that resolving long length scales in reconstructions of biogeochemical variables is of primary importance and provides a solid basis for the planning of the SOCCOM deployments [also in analysis by M. Mazloff personal communication, 2017]. Furthermore the idealized study demonstrates that float movement can improve spatial coverage and lower the RErr for the annual mean, while also degrading reconstruction of the seasonal cycle relative to the case with nonmoving floats [see also *Kamenkovich et al*., 2009, 2011]. Mesoscale variability in the sampled field can also increase RErr, especially in regions where its magnitude exceeds the magnitude of the seasonal cycle, such as the Agulhas region and the part of the ACC south of Australia. Reconstruction of the seasonal cycle in these regions requires high spatial sampling density, which is difficult to achieve due to fast movement of floats. Our results suggest that simple doubling of the number of floats from 150 to 300 is not sufficient for significant improvement of the reconstruction skill in these regions.

Conclusions from this study apply only to the reconstruction of global maps of upper ocean quantities. An observing system like SOCCOM can have additional, equally important objectives, including studying specific processes, regional properties, and water mass characteristics. These objectives will require separate analysis of carefully designed OSSEs. The numerical models used in our comprehensive OSSEs are among the most realistic available today, and most importantly, they have a high spatial resolution that allows at least partial resolution of mesoscale variability. The model-simulated fields can still have biases relative to the observed quantities, and conclusions from any OSSEs are potentially model specific. For example, model biases in temporal and spatial variability will undoubtedly affect the reconstruction skill and geographical distribution of RErr. Furthermore, the float trajectories used in our OSSEs were not calculated by the same model that produced the biogeochemical fields being reconstructed, which introduces additional uncertainty in our conclusions that needs to be addressed in future studies. This uncertainty will depend on how strongly the 1000 m trajectories are correlated with these fields, although the idealized model suggests that the dependence of RErr on the float advection speed is modest. We did not attempt to use OSSEs for optimization of the objective mapping technique used in this study or to study the dependence of the conclusions on its parameters. Our main goal was to establish the feasibility of the map reconstruction with an array of 150 floats and to study the primary factors affecting the resulting reconstruction skill. Note that both the size of the actual full SOCCOM array (150 floats) and its net lifespan (5 years) may be different from those used in the control simulation here. These important parameters are affected by the rate of loss of floats, float design, specific deployment strategy, and future extensions of the array that cannot be taken into account in our study.

Perhaps the largest source of uncertainty in these conclusions lies in the SOCCOM deployment sites and trajectories. To address this uncertainty and to reduce the potential model dependence in the results, we used an ensemble of real and model-simulated Argo trajectories. As the actual SOCCOM array is being gradually brought to full strength, most of the deployment sites are still to be determined. Conclusions from this study can be used to assist the deployment planning, by indicating regions where more profiles are needed, such as the ACC south of Australia, the SW Atlantic and the Agulhas. Further studies that focus specifically on the future deployments and the expected reconstruction errors are currently under way. Finally,

as the number of under-ice measurements by Argo-like floats has been recently growing, studies of the corresponding reconstruction skill are being carried out, with a focus on the importance of uncertainty in profile locations.

References

Arnold, C. P., Jr., and C. H. Dey (1986), Observing-system simulation experiment: Past, present and future, *Bull. Am. Meteorol. Soc.*, *67*, 687–695.

Ballabrera-Poy, J., E. Hackert, R. Murtugudde, and A. J. Busalacchi (2007), An Observing System Simulation Experiment for an optimal moored instrument array in the tropical Indian Ocean, *J. Clim.*, *20*, 3284–3299.

Barth, N., and C. Wunsch (1990), Oceanographic experiment design by simulated annealing, *J. Phys. Oceanogr.*, *20*, 1249–1263.

Bennett, A. F. (1990), Inverse methods for assessing ship-of-opportunity networks and estimating circulation and winds from tropical expendable bathythermograph data, *J. Geophys. Res.*, *95*, 16,111–16,148.

Delworth, T. L., et al. (2012), Simulated climate and climate change in the GFDL CM2.5 high-resolution coupled climate model, *J. Clim.*, *25*(8), 2755–2781, doi:10.1175/JCLI-D-11-00316.1.

Dufour, C. O., et al. (2015), Role of mesoscale eddies in cross-frontal transport of heat and biogeochemical tracers in the Southern Ocean, *J. Phys. Oceanogr.*, *45*, 3057–3081, doi:10.1175/JPO-D-14-0240.1.

Galbraith, E. D., et al. (2015), Complex functionality with minimal computation: Promise and pitfalls of reduced-tracer ocean biogeochemistry models, *J. Adv. Model. Earth Syst.*, *7*, 2012–2028, doi:10.1002/2015MS000463.

Gray, A. R., and S. C. Riser (2015), A method for multiscale optimal analysis with application to Argo data, *J. Geophys. Res. Oceans*, *120*, 4340–4356, doi:10.1002/2014JC010208.

Griffa, A., A. Molcard, F. Raicich, and V. Rupolo (2006), Assessment of the impact of TS assimilation from Argo floats in the Mediterranean Sea, *Ocean Sci.*, *2*, 237–248.

Griffies, S. M., et al. (2015), Impacts on ocean heat from transient mesoscale eddies in a hierarchy of climate models, *J. Clim.*, *28*(3), 952–977, doi:10.1175/JCLI-D-14-00353.1.

Hackert, E. C., R. N. Miller, and A. J. Busalacchi (1998), An optimized design for a moored instrument array in the tropical Atlantic Ocean, *J. Geophys. Res.*, *103*, 7491–7509.

Hernandez, F., P.-Y. Le Traon, and L. H. Barth (1995), Optimizing a drifter cast strategy with a genetic algorithm, *J. Atmos. Oceanic Technol.*, *12*, 330–345.

Kamenkovich, I., W. Cheng, E. S. Sarachik, and D. E. Harrison (2009), Simulation of the Argo observing system in a global ocean model, *J. Geophys. Res.*, *114*, C09021, doi:10.1029/2008JC005184.

Kamenkovich, I., W. Cheng, C. Schmid, and D. E. Harrison (2011), Effects of eddies on an ocean observing system with profiling floats: Idealized simulations of the Argo array, *J. Geophys. Res.*, *116*, C06003, doi:10.1029/2010JC006910.

Kindle, J. C. (1986), Sampling strategies and model assimilation of altimetric data for ocean monitoring and prediction, *J. Geophys. Res.*, *91*, 2418–2432.

Majkut, J. D., B. R. Carter, T. L. Frölicher, C. O. Dufour, K. B. Rodgers, and J. L. Sarmiento (2014), An observing system simulation for Southern Ocean carbon dioxide uptake, *Philos. Trans. R. Soc. A*, *372*, 20130046.

Nowlin, W. D., and J. M. Klinck (1986), The physics of the Antarctic Circumpolar Current, *Rev. Geophys.*, *24*, 469–491.

Orsi, A. H., T. Whitworth III, and W. D. Nowlin Jr. (1995), On the meridional extent and fronts of the Antarctic Circumpolar Current, *Deep Sea Res., Part I*, *42*, 641–673.

Schiller, A., S. E. Wijffels, and G. A. Meyers (2004), Design requirements for an Argo float Array in the Indian Ocean inferred from Observing System Simulation Experiments, *J. Atmos. Oceanic Technol.*, *21*, 1598–1620.

Vecchi, G. A., and M. Harrison (2007), An Indian Ocean Observing System Simulation Experiment, *J. Clim.*, *20*, 3300–3319.

Erratum

In the originally published version of this article, the modeling code DOI in the Acknowledgments section did not link to its online source. This DOI has since been updated and links to an online source, so this version may be considered the authoritative version of record.